The Chlamydia effector CT622/TaiP 3 targets a non-autophagy related function of ATG16L1 4 5

Daniel Hamaoui, Mathilde Cossé, Jagan Mohan, Alf Håkon Lystad, Thomas Wollert, Agathe Subtil

Classification: Biological Sciences

Title: The *Chlamydia* effector CT622/TaiP targets a non-autophagy related function of ATG16L1

Daniel Hamaoui[1], Mathilde M. Cossé[1], Jagan Mohan[2], Alf Håkon Lystad[3], Thomas Wollert[2] & Agathe Subtil[1#].

1. Unité de Biologie cellulaire de l'infection microbienne, Institut Pasteur, UMR3691 CNRS, F-75015, Paris, France.
2. Biochimie membranaire et transport, Institut Pasteur UMR3691 CNRS, F-75015, Paris, France.
3. Department of Molecular Medicine, Institute of Basic Medical Sciences and Centre for Cancer Cell Reprogramming, Institute of Clinical Medicine, Faculty of Medicine, University of Oslo, Norway.

Corresponding author. Email: asubtil@pasteur.fr Phone : +33 14061 3049

Keywords: host-pathogen interactions, autophagy, ATG16L1, intracellular traffic, *Chlamydia trachomatis*

Abstract

The obligate intracellular bacteria *Chlamydia trachomatis,* the causative agent of trachoma and sexually transmitted diseases, multiply in a vacuolar compartment, the inclusion. From this niche, they secrete “effector” proteins, that modify cellular activities to enable bacterial survival and proliferation. Here, we show that the host protein ATG16L1 restricts inclusion growth, and that this effect is counteracted by the secretion of the bacterial effector CT622/TaiP (Translocated ATG16-L1 interacting Protein). ATG16L1 is mostly known for its role in the lipidation of the human homologs of ATG8 (*i.e.* LC3 and homologs) on double membranes during autophagy, as well as on single membranes during LC3-associated phagocytosis and other LC3-lipidation events. Unexpectedly, the LC3 lipidation-related functions of ATG16L1 are not required for restricting inclusion development. We show that the carboxy-terminal domain of TaiP exposes a mimic of an eukaryotic ATG16L1-binding motif, that binds to ATG16L1’s WD40 domain. By doing so, TaiP prevents ATG16L1 interaction with the integral membrane protein TMEM59, and allows the rerouting of Rab6-positive compartments towards the inclusion. The discovery that one bacterial effector evolved to target ATG16L1’s engagement in intracellular traffic rather than in LC3 lipidation brings this “secondary” activity of ATG16L1 in full light, and emphasizes its importance for maintaining host cell homeostasis.

Significance statement:

Some intracellular bacteria develop inside a vacuole, which expands during the infection process. We show here that the protein ATG16L1 restricts the expansion of the *Chlamydia trachomatis* vacuole. ATG16L1 is well known for its role in autophagy, a process that contributes to the elimination of intracellular microbes. However, the restriction exerted by ATG16L1 on vacuole expansion relies on a different ATG16L1 function. We demonstrate that the bacteria secrete an effector protein that prevents ATG16L1 binding to TMEM59, and allows rerouting of vesicular traffic to the vacuole. The discovery that one bacterial effector evolved to target ATG16L1’s engagement in intracellular traffic emphasizes the importance this “secondary” activity of ATG16L1 for maintaining host cell homeostasis.

Introduction:

Chlamydia trachomatis is an obligate intracellular pathogen responsible for the most common sexually transmitted bacterial infection (1). The bacteria reside within a vacuolar compartment, called the inclusion, which expands throughout the developmental cycle. The host and the bacteria contribute collectively to the making of this compartment. In particular, host lipids are diverted to the inclusion membrane both through vesicular and non-vesicular traffic (2). The nature of the intercepted vesicles is not fully understood, and the presence of many different Rab GTPases at the inclusion membrane suggests that several trafficking pathways are involved (3). Key players in this rerouting of host-derived vesicles are the bacterial Inc proteins, that are inserted into the inclusion membrane, and that interact with regulators of intracellular traffic (4). However, Inc proteins are confined to the inclusion membrane, which limits their range of action. We recently observed that the loss of expression of the soluble effector CT622 in a *Ctr*$^{\Delta ct622}$ strain resulted in several deficiencies, including a defect in inclusion growth, supporting the hypothesis that this soluble effector might contribute to the diversion of host-derived material towards the inclusion (5). In the present study, we identify the host protein ATG16L1 as a target of CT622. ATG16L1 is best known for its role as part of the ATG12-ATG5-ATG16L1 complex, which catalyzes the lipidation of the human homologs of ATG8 (*i.e.* LC3 and homologs) on double membranes during autophagy, as well as on single membranes during LC3-associated phagocytosis and other LC3-lipidation events (6-9). ATG16L1 also plays an important role in the control of inflammation through its ability to bind NOD1 and NOD2 (10). Very unexpectedly, we show here that the ATG16L1-driven function that is targeted by CT622 is not related to its LC3 lipidation capacity, nor to its ability to bind NODs, but to its involvement in regulating intracellular traffic by interacting with the transmembrane protein TMEM59. We show that CT622 inhibits the formation of the ATG16L1/TMEM59 complex, allowing the rerouting of vesicular traffic to the inclusion, thereby rescuing inclusion growth in the *Ctr*$^{\Delta CT622}$ strain.

Results

CT622 binds to ATG16L1 through its carboxy-terminal domain

The observation that loss of CT622 impaired inclusion growth suggested that this soluble effector might contribute to the diversion of host-derived material towards the inclusion. To identify the targets

of CT622 in the host cytoplasm we performed two independent pull-down experiments. We identified 33 proteins that were significantly enriched in the GST-CT622 pulled-down fraction compared to GST, three of which being recovered in the two independent experiments (Table S1). The autophagy related (ATG) proteins ATG16L1 and ATG5 were recovered in the two experiments, with the highest total peptide counts. To test their ability to interact with CT622 we first performed co-immunoprecipitation experiments in cells transfected with plasmids expressing Flag-CT622, GFP-ATG5 and/or GFP-ATG16L1. After cell lysis, we immunoprecipitated Flag-CT622, separated the proteins by SDS-PAGE and probed this fraction with antibodies against GFP by western blot. GFP-ATG16L1 co-immunoprecipitated with Flag-CT622 while GFP-ATG5 did not (Fig1A). This result suggests that CT622 interacts with ATG16L1. The recovery of ATG5 in the pull-down but not in the co-immunoprecipitation suggests that, when all protein were expressed at the endogenous level, ATG5 co-fractionated with CT622 via its ability to bind ATG16L1. By immunofluorescence, we observed that co-expression of GFP-ATG16L1 with Flag-CT622 led to the relocation of Flag-CT622 to GFP-ATG16L1 puncta, further supporting the hypothesis that the two proteins interact (SI Appendix Fig. 1A).

CT622 exhibits a highly conserved carboxy-terminal domain ($CT622^{Cterm}$) and a somewhat less conserved amino-terminal domain ($CT622^{Nterm}$) (5). Co-immunoprecipitation experiments with each of these domains expressed individually revealed that the interaction with ATG16L1 occurred via $CT622^{Cterm}$ (Fig1B). To confirm this interaction in the context of an infection and in the absence of protein overexpression we used the $Ctr^{\Delta ct622}$ strain complemented with *ct622* with a carboxy-terminal Flag tag ($Ctr^{\Delta ct622+CT622\text{-}Flag}$), which we had characterized previously (5). Cells were infected for 35 h, lysed and anti-Flag antibodies were used to immunoprecipiate CT622-Flag. We detected endogenous ATG16L1 in the immunoprecipitated fraction, supporting the hypothesis that CT622 interacted with ATG16L1 in infection (Fig. 1C). Finally, to determine whether the interaction was direct, we incubated purified ATG16L1 with either recombinant GST-CT622 or recombinant $GST\text{-}CT622^{Nterm}$ as negative control. We pulled-down GST using glutathione-bound resin and measured the levels of ATG16L1 that co-purified in these fractions by quantifying band intensities in western blot. ATG16L1 co-purified with GST-CT622, demonstrating that the interaction between the two proteins was direct (Fig. 1D). Based on these data we propose to rename CT622 Translocated ATG16L1 interacting Protein (TaiP), which is consistent with the nomenclature for other soluble chlamydial effectors (*e.g.* TarP, TepP, TmeA).

ATG16L1 restricts *C. trachomatis* development and the restriction is exacerbated in the absence of TaiP.

To study the role of ATG16L1 in *C. trachomatis* infection, we generated *atg16l1* KO HeLa cells (Fig. 1E), in which we verified that LC3B lipidation was fully impaired (SI Appendix Fig. 1B). We compared the ability of wild type bacteria (*Ctr*^{WT}), *Ctr*$^{\Delta taiP}$ and *Ctr*$^{\Delta taiP+TaiP\text{-}Flag}$ to establish an infection in this cellular background compared to the parental HeLa cells. The loss of ATG16L1 resulted in a 20% increase in the size of the inclusions of *Ctr*^{WT} and *Ctr*$^{\Delta taiP+TaiP\text{-}Flag}$ (Fig. 1E), indicating that ATG16L1 restricts the development of *C. trachomatis*. Strikingly, the increase in inclusion diameter was much more pronounced (~ 70% increase) for the *Ctr*$^{\Delta taiP}$ strain. As a result, the *Ctr*$^{\Delta taiP}$ inclusions in the *atg16l1* background reached the average size for *Ctr*^{WT} in control cells (Fig. 1 E). The recovery in inclusion size was observed in four independent *atg16l1* KO clones, and is therefore not an clonal effect (SI Appendix Fig. 1C).The same observations were made when using siRNA targeting ATG16L1 in HeLa cells, as well as in the endometrial epithelial cell line HEC-1-B (SI Appendix Fig.1D-E). These data indicate that at least part of the decrease in inclusion growth observed in the *Ctr*$^{\Delta taiP}$ strain is due to its inability to counteract an ATG16L1-driven restriction on inclusion development. In support of this, we observed that the transfection of Flag-CT622 prior to infection resulted in a 50% increase in inclusion size for the *Ctr*$^{\Delta taiP}$ strain, and a 40% increase for the *Ctr*^{WT} strain (Fig. 1E). A construct expressing an irrelevant Flag-tagged protein (CymR) expressed at similar levels as Flag-TaiP, was used as a negative control. Altogether, we concluded from these series of experiments that ATG16L1 hinders inclusion development, and that one of the roles of the effector TaiP is to counteract this brake by binding to ATG16L1. Importantly, the absence of ATG16L1 resulted in a ~ two-fold increase in progeny for the *Ctr*$^{\Delta taiP}$ strain (SI Appendix Fig. 1F). This is modest compared to the 25-fold difference of infectivity that exists between the *Ctr*$^{\Delta taiP}$ and *Ctr*^{WT} strains (5), implicating that while the inclusions recovered a normal size, the other phenotype associated to TaiP loss, *i.e.* defect of infectivity of EBs, remained. This is not surprising, considering that the loss of progeny in the *Ctr*$^{\Delta taiP}$ strain is largely due to the formation of non-functional EBs (*e.g.* defects in TarP secretion for instance), which is likely disconnected from the defect on the inclusion size. The absence of ATG16L1 did not significantly affect the progeny of the *Ctr*^{WT} or *Ctr*$^{\Delta taiP+TaiP\text{-}Flag}$ strains (SI Appendix Fig. 1F).

ATG16L1 restricts inclusion growth through its WD40 domain

ATG16L1 amino-terminal part is structurally and functionally conserved in yeast and is responsible for its role in LC3 lipidation. Its carboxy-terminal part is made of an unstructured region followed with seven WD40 repeats (amino acids 320 to 607) and is absent in the yeast ortholog (Fig. 2A). The seven WD40 repeats form part of a beta-propellar domain which recruits several ATG16L1 effector proteins including NOD1, NOD2 and TLR2 (11-13). Notably, while the WD40 domain is dispensable for LC3 lipidation on double membrane autophagosomes during classical autophagy, it was shown to be required for ATG12-ATG5-ATG16 complex-mediated LC3 lipidation at single membranes (7, 9). To investigate the mechanism by which ATG16L1 restricts inclusion development we expressed in wild-type or *atg16l1* KO HeLa either GFP, full length GFP-ATG16L1 (GFP-ATG16L1^{FL}), a truncated form of ATG16L1 lacking the WD40 domain (GFP-ATG16L1$^{1-319}$), or a truncated form of ATG16L1 lacking the ATG5-binding and coiled-coil domains (GFP-ATG16L1$^{266-607}$). As expected, expression of GFP-ATG16L1^{FL} and of GFP-ATG16L1$^{1-319}$ in *atg16l1* KO cells rescued LC3B lipidation, and GFP-ATG16L1$^{266-607}$ did not (SI Appendix Fig. 2A). These cells were infected with *Ctr*$^{\Delta taiP}$, and the median size of inclusions in the GFP-positive cells was measured (SI Appendix Fig. 2B). We observed that the expression of GFP-ATG16L1^{FL} and GFP-ATG16L1$^{266-607}$ decreased the size of the *Ctr*$^{\Delta taiP}$ inclusions compared to GFP expressing cells, whereas the expression of GFP-ATG16L1$^{1-319}$ did not (Fig. 2B). These experiments demonstrate that the E3-ligase activity of ATG16L1 is dispensable for the restriction this protein exerts on *C. trachomatis* development. Interestingly, the presence of LC3B at the inclusion periphery had been reported in a previous study, and the authors had concluded that this observation did not depend on a functional autophagy machinery (14). In agreement with that report, we observed an enrichment of LC3B around the inclusion, labeled with an antibody against the inclusion protein Cap1 (Fig. 2C). Strikingly, the presence of LC3B around the inclusion was independent of the LC3B lipidation by the ATG12-ATG5-ATG16 complex since it was also observed in *atg16l1* KO HeLa cells (Fig. 2C), or in *atg16l1* KO or *atg3* KO HEK293 cells (Fig S2B). It was also independent of the expression of TaiP, as *Ctr*$^{\Delta taiP}$ inclusions were also decorated with LC3B (Fig. 2C). Thus, while the presence of LC3B at the inclusion membrane is an intriguing observation, we concluded from these experiments that it is not related to the TaiP/ATG16L1 interaction.

Since the expression of the WD40 domain was sufficient to restrict the growth of *Ctr*$^{\Delta taiP}$ inclusions we tested whether this domain was implicated in the interaction between ATG16L1 and TaiP. Purified

GST-CT622 was incubated with lysates from *atg16l1* KO cells expressing either GFP-ATG16L1$^{1-319}$ or GFP-ATG16L1^{FL}, before purifying GST-TaiP together with associated proteins (Fig. 2D). We worked in an *atg16l1* KO background to avoid possible dimerization of the expressed constructs with endogenous ATG16L1. ATG16L1^{FL} co-purified with GST-TaiP while ATG16L1$^{1-319}$ did not, indicating that the WD40 is necessary for the formation of the TaiP/ATG16L1 complex (Fig. 2D). Consistent with this result, we observed that Flag-TaiP no longer relocalized to GFP-ATG16L1 puncta in the absence of the WD40 (Fig. 2E). Altogether, we concluded from these experiments that TaiP targets the WD40 domain of ATG16L1. This interaction results in a gain in inclusion growth through a pathway that does not require the LC3-lipidation capacity of ATG16L1.

TaiP promotes inclusion growth by disrupting ATG16L1/TMEM59 interaction.

To identify the ATG16L1-related complex or pathway that is targeted by TaiP we reasoned that silencing the expression of proteins involved in this process should result in the same phenotype as ATG16L1 silencing, *i.e.* a rescue of the growth of the *Ctr*$^{\Delta taiP}$ strain. We thus transfected cells with siRNA against the five best characterized binding partners of the WD40 domain of ATG16L1, TLR2, NOD1, TMEM59, T3JAM and DEDD2 (12). NOD2 was not tested as it is not expressed in HeLa cells. siRNA against ATG16L1 was included in the screen as a positive control, and the efficiency of the silencing was verified by qRT-PCR (SI Appendix Fig. 3A). Thirty hours later, the cells were infected with *Ctr*$^{\Delta taiP}$. The cells were fixed 20 hrs after infection and processed for measuring the size of the inclusions by immunofluorescence. We observed that silencing the expression of the protein TMEM59 phenocopied the phenotype observed with ATG16L1 silencing, *i.e.* an increase in the size of *Ctr*$^{\Delta taiP}$ inclusions (Fig. 3A), a result we confirmed in the HEC-1-B epithelial cell line (SI Appendix Fig. 3B). To avoid the possible sampling bias inherent to microscopy quantification we measured the percentage of infected cells detected by flow cytometry. When working at low MOI, this parameter is directly linked to bacterial load, because only cells bearing sufficient bacteria are recorded as infected (15). We observed that silencing the expression of the protein TMEM59, but not of the other proteins tested, significantly increased the percentage of infected cells, confirming the results obtained on inclusion size measurement (SI Appendix Fig. 3C). These results indicate that the restriction ATG16L1 exerts on the growth of *C. trachomatis* inclusions depends on its ability to interact with TMEM59. To strengthen this hypothesis, we tested whether TaiP interfered with the formation of ATG16L1/TMEM59

complexes. We first confirmed, using HeLa cells expressing GFP-ATG16L1 and HA-TMEM59, that the two proteins co-immunoprecipitate (Fig. 3B). When the immunoprecipitation was performed on cell infected with *Ctr*^{WT} or *Ctr*$^{\Delta taiP+TaiP\text{-}Flag}$ strains, we observed a decrease in the amount of ATG16L1 that co-immunoprecipitated with TMEM59. In contrast, infection with *Ctr*$^{\Delta taiP}$ did not prevent the interaction of ATG16L1 with TMEM59 (Fig. 3B). This result stongly supports an inhibitory role of TaiP on the formation of an ATG16L1/TMEM59 complex. To confirm these data,we expressed separately HA-TMEM59 and GFP-ATG16L1 in HeLa cells by transfection, then mixed cell lysates in the presence of purified GST-TaiP. GST-TaiP^{Nterm} was used as negative control in this assay since it does not bind to ATG16L1 (Fig. 1B). After incubation, HA-TMEM59 was immunoprecipitated, and we analyzed by western blot the levels of GFP-ATG16L1 in this fraction. In the presence of GST-TaiP^{Nterm} GFP-ATG16L1 co-immunoprecipitated together with HA-TMEM59. However, in the presence of GST-TaiP, the quantity of GFP-ATG16L1 that co-precipitated with HA-TMEM59 amounted to the signal observed in the absence of expression of HA-TMEM59, and thus corresponded to non-specific GFP-ATG16L1 binding to the beads (Fig. 3C). Interestingly, addition of GST-TaiP did not compromise the ability for ATG16L1 to interact with NOD1, NOD2 nor TLR2 (SI Appendix Fig. 3D). Thus, TaiP blocks specifically TMEM59/ATG16L1 interaction in epithelial cells.

TaiP mimics a eukaryotic domain for binding to ATG16L1 WD40 domain and D480 is a critical residue for TaiP/ATG16L1 interaction

Our results indicate that TaiP targets the ATG16L1/TMEM59 complex. TMEM59 is type I transmembrane protein whose role is poorly understood. Initially described as residing in the Golgi apparatus, it was later described as a player in endocytic trafficking from late endosomes to lysosomes, with a clear colocalization with lysosomal markers (12, 16). Overexpression of TMEM59 induced LC3 lipidation of the compartment in which the protein resides, through its ability to attract ATG16L1 (12). The Pimentel-Muiños' laboratory identified in its short cytoplasmic tail a WD40 binding motif defined as [YW]-X3-[ED]-X4-[YWF]-X2-L (12). This motif was found in several other proteins that bind to ATG16L1, such as TLR2 and the CARD domain of NOD2. We analysed TaiP sequence, and found a single matching motif **Y**^{474}AAALS**D**^{480}GYSA**Y**^{485}KT**L**^{488}, that corresponds to the 6th helix of TaiP^{Cter}, which is well exposed at the surface of the protein (5). To test whether this motif was implicated in ATG16L1/TaiP interaction we mutated aspartate 480 into an alanine (D480A). Co-

immunoprecipitation experiments showed that the introduction of this point mutation reduced the ability for TaiP to interact with ATG16L1 by about 50% (Fig. 3D). To confirm the engagement of this motif in ATG16L1/TaiP interaction we next measured the gain in inclusion size in HeLa cells transfected with either TaiP or TaiP^{D480A}, and infected with *Ctr*$^{\Delta taiP}$. Transfection of an irrelevant Flag-tagged construct, Flag-CymR, was used as a negative control. As previously observed, expression of TaiP resulted in increased *Ctr*$^{\Delta taiP}$ inclusion size. However, the mutated form of TaiP was unable to rescue inclusion growth (Fig. 3E). We concluded from these experiments that TaiP^{Cterm} 6th helix mimics the ATG16L1 binding motif [YW]-X3-[ED]-X4-[YWF]-X2-L, thereby allowing the bacterial effector to disrupt TMEM59/ATG16L1 interaction and favor inclusion growth.

TaiP diverts Rab6 and ATG16L1-dependent vesicular traffic towards the inclusion

We next analysed TMEM59 localisation in *Ctr*^{WT} and *Ctr*$^{\Delta taiP}$ infected HeLa cells. We observed TMEM59 in punctate structures, with no enrichment at the inclusion membrane, neither in cells infected with wild-type nor with *Ctr*$^{\Delta taiP}$ bacteria (SI Appendix Fig. 4). Our data show that silencing ATG16L1 or TMEM59 converge to a similar phenotype, *i.e.* a rescue of the growth of *Ctr*$^{\Delta taiP}$ inclusions. One possible explanation for this phenomenon is that in the absence of those players (or in the presence of TaiP, that disrupts their interaction), a pool of vesicles becomes available for inclusion growth. To strengthen this scenario, we looked for a molecular marker associated with such a pool of vesicles. Among the proteins that were significantly enriched in the GST-TaiP pull-down compared to GST alone (Table S1) we had identified several small Rab GTPases: Rab5, Rab7 and small GTPases that could not be identified because the peptide recovered was common to several Rab proteins (Rab6, 27, 34, 39, 41 and 44). Out of these potential candidates, Rab 6 and Rab39 are recruited to the chlamydial inclusion, (17, 18). Furthermore, silencing Rab6 reduces the delivery of the lipid ceramide to the inclusion (19). To test if TaiP was able to interact with Rab proteins as indicated by the mass spectrometry data we performed co-immunoprecipitation experiments in cells co-transfected with flag-tagged TaiP and GFP-tagged Rab proteins. We tested several of the Rab proteins that the pull-down assay had hinted to as potential interactors (Rab 5, 6, 7, 39), as well as Rab14 because it is one of the Rab proteins recruited to the inclusion membrane (20). TaiP co-immunoprecipitated with Rab6a and Rab39a, and with none of the other Rab proteins tested (Fig. 4A). Deletion of the carboxy-terminal domain of TaiP abolished these interactions, indicating that this domain is involved (Fig. 4B). To

determine if the growth defect of the *Ctr*$^{\Delta taiP}$ strain was due to an inability to mobilize Rab6 or Rab39-regulated vesicular traffic, we tested the effect of silencing Rab6 or Rab39 on bacterial development. Silencing Rab39 had no effect on the ability for the bacteria to infect and grow in HeLa cell, and this small GTPase was not investigated further. Silencing of Rab6 resulted in a 25 % decrease in the inclusion size of wild type bacteria, confirming its role in feeding *Chlamydia*-inclusion growth (19) (Fig. 4C). In contrast, depleting Rab6 had no significant impact on the size of *Ctr*$^{\Delta taiP}$ inclusions. This result suggests that the TaiP/ATG16L1-dependent vesicular traffic that contributes to the growth of the inclusion in the wild-type strain requires Rab6. To further link Rab6 to the TaiP/ATG16L1 dependent growth of *Chlamydia* inclusions we looked at the consequence of silencing Rab6 in the wild-type versus the *atg16l1* KO background. We observed that the benefice, for the *Ctr*$^{\Delta taiP}$ strain, of knocking-out ATG16L1 expression was lost when Rab6 was silenced (Fig. 4C). This observation indicates that the source of membrane that allows faster growth of the *Ctr*^{WT} strain compared to the *Ctr*$^{\Delta taiP}$ strain is Rab6 dependent. Rab6 is highly enriched in the Golgi apparatus, which is localized close to the inclusion (SI Appendix Fig. 4). To facilitate the quantification of vesicular Rab6 enrichment at the inclusion periphery we applied a short treatment with nocodazole, an inhibitor of microtubule polymerization, that results in the dispersion of Golgi stacks (21). Infected cells were fixed and stained for endogenous Rab6 and for the inclusion protein CT813 (Fig. 4D). We observed a stronger enrichment in Rab6 at the periphery of *Ctr*$^{\Delta taiP}$ inclusions compared to *Ctr*$^{\Delta taiP}$, an observation fully consistent with the hypothesis that TaiP is required for efficient recruitment of Rab6 positive vesicles to the inclusion. Furthermore, the recruitment of Rab6 to *Ctr*$^{\Delta taiP}$ inclusions, but not to *Ctr*^{WT} inclusions, increased significantly in the *atg16l1* KO background, indicating that ATG16L1 restricts Rab6 traffic towards the inclusion in the absence of TaiP (Fig. 4D). Altogether, our data converge to establish that one the functions of the chlamydial effector TaiP is to disrupt ATG16L1/TMEM59 interaction, through mimicry of WD40-binding motif. This unleashes access to a Rab6-dependent supply of membrane, that feeds inclusion growth (Fig. 5A). Our model predicts that Rab6-positive vesicles normally feed TMEM59-positive compartments, and that this pathway requires ATG16L1/TMEM59 interaction. The large overlap of Rab6 and TMEM59 positive compartments observed by immunofluorescence is consistent with this prediction (SI Appendix Fig. 4). To test it further we co-expressed GFP-Rab6 and HA-TMEM59 in wild type and in the *atg16l1* KO background. We observed that indeed Rab6 co-immunoprecipitated with TMEM59 in the wild type HeLa but not in the absence of ATG16L1 (Fig. 5B).

Thus, our study has uncovered a novel trafficking pathway, controlled by ATG16L1, that feeds TMEM59 positive compartments with Rab6-positive material.

Discussion

The observation that the absence of expression of TaiP resulted in several developmental defects had led us to hypothesize that this effector may contribute to multiple key events in infection (5). In this report, we show that the carboxy-terminal part of TaiP is engaged in the regulation of membrane supply to the inclusion, accounting for the defect in inclusion growth of the *Ctr*$^{\Delta taiP}$ strain. At the molecular level, we demonstrated that TaiP interacted with the host protein ATG16L1 through its C-terminal domain. Moreover, we found that TaiP competitively inhibited the interaction of TMEM59 and ATG16L1, *in vitro* and in the infectious context. Remarkably, silencing either TMEM59 or ATG16L1 expression allows to revert the inclusion growth defect of the *Ctr*$^{\Delta taiP}$ strain.

Most work on ATG16L1 has focused on its role in ATG8 lipidation as part of the ATG12-ATG5-ATG16 complex. We observed that silencing *atg16l1*, or disrupting its expression, enhanced *Chlamydia* growth, even for the wild-type strain. This observation led us to hypothesize that ATG16L1 might restrict *Chlamydia* growth through an autophagy-related mechanism. However, we demonstrated that it was not the case since the N-terminal part of ATG16L1, required and sufficient for ATG8 lipidation, was not able to restrict *Chlamydia* growth. Conversely, expression of the C-terminal part of ATG16L1, that contains the WD40, was sufficient for that effect. Therefore, the restriction of bacterial growth exerted by ATG16L1 is not due to its ability to mediate ATG8 lipidation, but is provided by a separate function of the WD40 domain.

ATG16L1's WD40 domain is proposed to interact with a variety of proteins (13, 22). A motif common to several ATG16L1 binding proteins had been identified as [YW]-X3-[ED]-X4-[YWF]-X2-L (12). TaiP^{Cterm} contains a single sequence that matches this definition: **Y**^{474}AAALS**D**GYSA**Y**KT**L**^{488}, and we showed that the D480A mutation impaired TaiP binding to ATG16L1. Thus, our data confirm the privileged interaction between the [YW]-X3-[ED]-X4-[YWF]-X2-L motif and ATG16L1 WD40. Interestingly, the interaction between ATG16L1 and TLR2 or NOD2, which also carry the [YW]-X3-[ED]-X4-[YWF]-X2-L motif, appear insensitive to the addition of TaiP. This might be explained by difference in affinities and/or by the limitation of our read-out (co-immunoprecipitation), that might not be sensitive enough to reveal competition between these ATG16L1 binders. Also, other surfaces are

likely also implicated in the interactions between these different molecules and ATG16L1, as exemplified by NOD1, which binds ATG16L1 but does not present the motif (12). These additional binding surfaces could compensate for the competition exerted by helix 6 of TaiP.

We observed that exogenous expression of TaiP (by transfection) partially reverted the inclusion size defect of the *Ctr*$^{\Delta ct622}$ strain. Importantly, TaiP D480A point mutation abolished both the beneficial effect of TaiP expression on inclusion growth, and the disruptive effect of TaiP on ATG16L1/TMEM59 complexes, strongly supporting the hypothesis that TaiP supports *C. trachomatis* growth by disrupting ATG16L1/TMEM59 interaction. In favor of this scenario, we showed that TMEM59 silencing led to a similar phenotype as ATG16L1 silencing, *i.e.* a recovery of *Ctr*$^{\Delta taiP}$ inclusion size. TMEM59 is a transmembrane protein associated to several compartments, including the Golgi apparatus and late endocytic compartments, but its role in membrane traffic remains unclear. Our results converge to the hypothesis that ATG16L1/TMEM59 interaction limits bacterial access to host vesicular traffic (Fig. 5A). Translocation of TaiP disrupts ATG16L1/TMEM59 interaction, unleashing access to a membrane pool, that feeds inclusion growth. TaiP was detected by immunofluorescence in the bacteria throughout the developmental cycle, and in the cytosol late in the cycle, probably due to a detection threshold (5). Our new data are consistent with a role of TaiP throughout the inclusion growth phase, and in particular in the first half of the developmental cycle, when the difference in inclusion sizes compared to wild-type inclusions is the strongest. We showed that the ability of this membrane pool to support inclusion growth was dependent on the expression of the small GTPase Rab6. Rab6 is associated to several exocytic pathways emerging from the Golgi apparatus (23). Our data confirm the role of Rab6 in feeding *Chlamydia*-inclusion growth (19), and revealed the control, by ATG16L1, of a Rab6-positive membrane flow towards TMEM59 compartments.

ATG16L1 has attracted a lot of attention since the identification of an amino acid substitution (T300A) that sensitizes the protein to caspase-3 processing, and that is associated with diminished autophagy and increased risk of developing Crohn disease (24, 25). The molecular links between this variant and the susceptibility to Crohn disease are still unclear (26), and could involved impaired trafficking events (8, 27). The finding that ATG16L1T300A protein functions as a dominant negative raises the possibility that the cleavage products have deleterious activity of their own (28). The cleavage site liberates the WD40 domain, that we show here to be implicated in the control of the traffic of at least a subset of Rab6 positive vesicles. The fact that evolution shaped a bacterial effector

that targets this WD40 domain in order to redirect intracellular traffic to the bacterial compartment indicates that the role played by WD40 in this process is very central. Future work will thus need to consider the possibility that impaired ATG16L1-controled trafficking events could play a major role in the susceptibility to Crohn disease, and other pathologies in which ATG16L1 has been implicated.

Methods:

Cells and bacteria.

HeLa (ATCC), HEC-1-B (ATCC) and HEK293 cells (Invitrogen) were grown in Dulbecco's modified Eagle's medium with Glutamax (DMEM, Invitrogen), supplemented with 10 % (v/v) heat-inactivated fetal bovine serum (FBS). HEK293 *atg3* KO and *atg16l1* KO cells used for SFig. 2 were described in (9). *C. trachomatis* serovar LGV L2 strain 434 (Ctr^{WT}) and the *taiP* genetic disruption mutant $Ctr^{\Delta taiP}$ mutant were propagated on HeLa cells as described (5).

Generation of *atg16l1* KO HeLa cells.

The *atg16l1* KO HeLa cells were generated as described in (29), inserting sgRNA CACCGCTGCAGAGACAGGCGTTCG (forward) and AAACCGAACGCCTGTCTCTGCAGC (reverse) in the pSpCas9(BB)-puro. After transfection, the cells were treated with 0.5 µg/ml puromycin for 24 h before individual clone selection. After monoclonal expansion, the loss of ATG16L1 expression was verified by western blot. All experiments with cells passaged 4 times or less after freezing.

Pull-down of GST-TaiP partners in infected and non-infected cells and mass spectrometry

HeLa cells (about 10^7 cells per point), infected or not for 24 hrs with *C. trachomatis,* were lysed in 0.05% NP40 lysis buffer with gentle rocking at 4 °C (150 mM NaCl, 50 mM Tris-HCl pH 7.5, 1 mM EDTA, 1 mM EGTA, 10 mM NaF, 5% glycerol supplemented with 0.5% NP40 (v/v)) for the first 20 min of lysis in a 0.1 ml volume, and diluted 1:10 to reach 0.05% NP40 for the last 20 min of lysis, and the rest of the procedure. Lysates were centrifuged at 17000 x*g* for 15 minutes at 4 °C and precleaned with glutathione-agarose beads with 20 µg of GST for 90 minutes at 4 °C in a rocking platform. Equal amount of precleaned supernatants were incubated with 50 µl of a 50 % slurry of glutathione sepharose 4B beads and 30 µg of purified GST or GST-TaiP for 90 min at 4 °C, on a rocking platform. After a brief centrifugation, beads were washed five times with cold GST lysis buffer. The bound proteins were eluted with urea buffer (8M urea, 1% SDS, 150 mM NaCl, 30 mM Tris-HCl pH 8.0) then identified by mass spectrometry by the Proteopole of the Institut Pasteur as described in (5).

Recombinant protein purification

GST-TaiP (GST-CT622) purification was described in (5). The same protocol was used to produce GST-TaiP^{Nterm}. ATG16L1 cDNA was cloned into pCoofy 29 vector via Sequence and Ligation Independent Cloning. ATG16L1 protein was expressed in H5 insect cells grown in EX-CELL 420 serum-free medium (Sigma-Aldrich). Baculovirus-infected insect cells were added in a ratio of 1:1000. Cultures were shaken for 72 hrs at 25°C and 85 rpm. Insect cells were harvested by centrifugation at 2000 x *g* for 15 min, washed with Dulbecco's phosphate buffered saline (Gibco) and resuspended in lysis buffer (0.1M Tris-HCl pH 8.0, 0.5M NaCl, 20mM imidazole, pH 8.0 , 10% glycerol, 5mM β-mercaptoethanol, 0.5% protease inhibitor cocktail (Sigma)). Cells were lysed using a dounce homogenizer. ATG16L1 was purified from cell lysates using a His-trap Ni-NTA agarose column followed by gel filtration in Superdex 200 column. His tag was removed by preScission protease and the released protein was subjected to size exclusion chromatography. Fractions containing ATG16L1 were pooled and concentrated using Vivaspin cellulose centrifugation filters (Sartorius Stedim). The protein was flash frozen in liquid nitrogen and stored at -80°C.

***In vitro* assay of ATG16L1/TaiP interaction and immunoblots**

GST-TaiP and GST-TaiP^{Nterm} at 100 µM were incubated with ATG16L1 at 33 µM, in the binding buffer (0.4 M NaCl, 25mM Tris-HCl, pH 7.4) and rocked on an Eppendorf tube roller for 2 h at 4°C. Pre-washed 30 µl slurry Glutathione–Sepharose-4B beads were then added to the protein mix and further incubated for 40 min at 4°C. The beads were centrifuged at 1500x*g* for 5 min and more than 90% of the supernatant was removed. The sedimented beads were washed twice in binding buffer supplemented with 0.1% Triton X-100 and once in binding buffer. The samples were eluted by boiling in SDS sample buffer and analyzed by immunoblotting. Immunoblots were analyzed using horse-radish peroxidase secondary antibodies and chemiluminescence was analyzed on a Syngene Pxi4 imaging system. For the quantification the background signal was subtracted from all bands before calculating the fold enrichment to the indicated control.

LC3B-PE turnover measurement

1.5*10^5 WT and *atg16l1* KO HeLa cells were seeded in duplicate 12 well-plates for each condition. The following day they were treated with vehicle (DMSO - D2650 Sigma) or 10 nM bafilomycinA1 (Sigma B1793). Three hours later, the cells were washed with PBS before lysis with Laemmli buffer supplemented with 2% ß-mercaptoethanol and boiled for 5min. The lysats were

separated by electrophoresis on SDS-PAGE at 15% acrylamide concentration before being transferred to a PVDF membrane. LC3B and LC3B-PE were revealed using the antibody NB100-2220 from Novus Biologicals.

Plasmids and transfections

Genomic DNA from *C. trachomatis* D/UW-3/CX, was prepared from bacteria using the RapidPrep Micro Genomic DNA isolation kit (Amersham Pharmacia Biotech). attB-containing primers (Table S2, Gateway®, Life technologies) were used to amplify and clone *ct622* into a destination vector derived from the mammalian expression vector pCiNeo, providing an amino-terminal 3xflag tag, and into pDEST15 (Gateway), for production of GST-tagged proteins. All constructs were verified by sequencing. EGFP-conjugated ATG16L1β constructs (WT and GFP-ATG16L1$^{266-607}$) were from Dr. E. Morel (INEM, Paris), TMEM59 was Dr. S Lichtenthaler (TUM, Germany), Flag NOD1/2 constructs we're from Dr. L Boyer (University of Nice) and TLR2 from Dr. P Cossart (Institut Pasteur, France), GFP-Rab6 was from B. Goud's laboratory (Institut Curie, France), GFP-Rab5 was obtained from A. Echard (Pasteur Institute), and GFP-Rab7, GFP-Rab14, GFP-Rab39 were kindly provided by M.T. Damiani (Mendoza, Argentina). Single point mutagenesis was performed to generate Flag-TaiP^{D480A} and GFP- GFP-ATG16L1$^{1-319}$ using the Quickchange Lightning Site-Directed Mutagenesis Kit from Agilent following the manufacturer's protocol and primers reported in Table S2.

DNA transfection were performed using Jet prime and following the manufacturer's protocol. For siRNA transfection we used RNAi Max as recommended by the manufacturer (see Table S2 for sequences).

Immunofluorescence

1.5*10^5 HeLa cells were seeded on glass cover slips in 12 well plates, before transfection (for expression of Flag-tagged proteins or for silencing) for 24h. Transfected cells were then infected for 20 hrs at a multiplicity of infection (MOI)=0.2, before fixation with 4% paraformaldehyde (PFA) in PBS for 20 min, followed with 10 min quenching with 50 mM NH_4Cl, in PBS. The cells were washed with PBS, permeabilized with 0.05% saponin, 5 mg/ml BSA in PBS (permeabilization buffer) for 20 min, and immunolabelled for 60 min with primary antibodies diluted in permeabilization buffer. Rabbit antibodies against the bacterial inclusion protein Cap1 are described in (30), mouse antibodies against CT813 were kindly provided by Dr. G. Zhong (San Antonio, Texas), mouse antibodies against LC3B were from MBL (#M152-3), antibodies against Flag(M2) were from Sigma, rat antibodies against TMEM59

(clone 4E5) were generously provided by Dr. S Lichtenthaler (16). Coverslips were then washed 3 times with PBS before incubating for 60 min in fluorochrome-coupled secondary antibodies diluted in permeabilization buffer. DNA was stained using 0.5 µg.mL^{-1} of Hoechst 33342 (Thermo Fisher Scientific) added in the secondary antibody solution. Images were acquired on an Axio observer Z1 microscope equipped with an ApoTome module (Zeiss, Germany) and a 63× Apochromat lens. Images were taken with an ORCAflash4.OLT camera (Hamamatsu, Japan) using the software Zen. Quantification of LC3B and Rab6 at the inclusion periphery were performed using the brush tool of ImageJ set, at 9 pixels, and following the inclusion membrane marker (Cap1 and CT813 respectively). To measure Rab6 enrichment at the inclusion periphery, the mean green fluorescence (Rab6) along the this line was normalized to the mean value of green fluorescence in two randomly selected ~ 1 µm^2 areas in the cytosol. Since LC3B level in the cytosol was hardly above background, this normalization was not applied for LC3B measurements and the data in Fig. 2C display the mean green (LC3B) fluorescence along the inclusion membrane.

Inclusion size measurements:

1.5*10^5 HeLa cells were seeded in 12 well-plates before transfection with either DNA or siRNA for 24 hrs. The transfected cells were infected in triplicates at MOI=0.2 for 20 hrs before being fixed and permeabilized for immunofluorescence. The inclusion membrane was stained using an antibody against Cap1 and 5 to 10 random pictures were taken for each coverslips as described in the immunofluorescence methods. Using the imageJ software the scale was set from pixels to µm and the area of individual inclusions were measured. Each condition was analyzed in a blind fashion from 3 individual coverslips with a minimum of 50 inclusions per simplicate. For Fig 1D, 3C, 4D & SFig1C the size of all inclusions was analyzed, whereas in Fig 1E & 3B the inclusions of only cells positive for Flag were analysed. For Fig2B only inclusions in GFP positive cells were taken into account and were analyzed. Note that we consistently observed that the inclusions grew slower in transfected cells compared to non transfected cells (compare for instance the average diameter of inclusions for *Ctr*^{WT} in non-transfected cells in Fig.1D and in cells transfected with GFP in Fig. 2B).

Progeny assay and flow cytometry

For progeny assays displayed in SFig. 1F wild-type or *atg16l1* KO HeLa cells infected for 40 h with the indicated strains were detached, lysed using glass beads and the supernatant was used to infect fresh HeLa cells plated the day before (100 000 cells/well in a 24-well plate), in serial dilution. The

next day, 3 wells per condition with an infection lower than 30 % (checked by microscopy) were detached, fixed in 70% ethanol and stained with a home-made rabbit antibody against GroEL followed with Alexa488-coupled secondary antibodies. Acquisition was performed using a CytoFLEX S (Beckman Coulter) and 10 000 events per sample were acquired and then analyzed using FlowJo (version 10.0.7) to determine the bacterial titer as described in (15). For determining the consequence of infection on bacterial load in SFig 3C, only the primary infection was analyzed by flow cytometry, after staining the bacteria with anti-GroEL antibodies.

Immunoprecipitation

5*10^6 HeLa cells were seeded in 10 cm^2 dishes. On the following day, cells were transfected with 5 µg of plasmid. One day later, cells were lysed in 250 µl of lysis buffer (150 mM NaCl, 50 mM Tris-HCl pH 7.5, 5% glycerol, 0.5% NP-40) supplemented with a protease cocktail inhibitor (Roche Complete, EDTA-free). The lysates were incubated on a rotating wheel at 4 ^oC for 20 min before adding 1ml of dilution buffer (150 mM NaCl, 50 mM Tris- HCl pH 7.5 supplemented with Protease cocktail inhibitor) thereby reducing the glycerol to 1% and NP-40 to a final concentration of 0,1%. The lysates were then centrifuged at 10,000 x*g* for 10 min and the insoluble pellet was discarded. For GFP IP the lysates were then incubated with 2 µg of antibody (Invitrogen, # A11122) at 4 ^oC for 2 hrs before adding 20 µl of slurry protein G beads (Sigma Fast Flow Protein G Sepharose) for 20 min. For HA and Flag IPs, antibody-coupled beads were used (Sigma). The beads were then washed before adding 20 µl of Laemmli buffer supplemented with 2% ß-mercaptoethanol and boiled for 5 min. For Fig1A, 1B the plasmids were co-transfected, whereas for Fig 3C an SFig3 A to C, the plasmids were transfected individually before mixing 0.75 ml of each diluted lysats in the presence or absence of 100 pmol of GST-$TaiP^{Nterm}$ or GST-TaiP. For the immunoprecipitation in infected cells shown in Fig. 1C cell lysis was performed in RIPA buffer (150 mM sodium chloride, 0.5% NP-40 and 0.5 Triton X-100, 0.5% sodium deoxycholate, 0.1% sodium dodecyl sulfate and 50 mM Tris, pH 8.0). Antibodies used for probing the membranes are descrived in the immunofluorescence section, in addition antibodies againstGFP (#NB600-308), ATG16L1 (#PM040) and HA (clone 12CA5) were purchased from Novus, MBL and Sigma, respectively.

Pull down assays

2.5*10^6 HeLa cells were seeded in 6 cm^2 dish the day before transfection with 2.5 µg of plasmid. On the following day, the cells were lysed in 250 µl of lysis buffer (150 mM NaCl, 50 mM Tris- HCl pH

7.5, 5% glycerol, 0.5% NP-40) supplemented with a protease cocktail inhibitor (Roche Complete, EDTA-Free). The lysates were incubated on a rotating wheel at 4 ^{o}C for 20 min before reducing the glycerol to 1% and NP-40 to a final concentration of 0.1% as above. The lysates were then incubated with 100 pmol of GST-TaiP for 60 min on a spinning wheel at 4 ^{o}C before adding 30 µl of slurry Glutathione-sepharose beads for 20 min. The beads were then washed 3 times using lysis buffer before adding 20 µl of Laemmli buffer supplemented with 2% ß-mercaptoethanol, and boiled for 5min.

RT-qPCR

Total RNAs were isolated 35 h after transfection with the RNeasy Mini Kit (Qiagen) with DNase treatment (DNase I, Roche). Reverse transcription was performed on 500 ng of total RNA using the high capacity c-DNA Reverse transcription kit (Applied Biosystems) according to manufacturer's instructions. Complementary DNA (cDNA) were diluted 5 times and quantitative PCR (qPCR) was performed on 1 µl of cDNA with the LightCycler 480 system using LightCycler 480 SYBR Green Master I (Roche). Data were analyzed using the $\Delta\Delta$Ct method with the 36B4 gene as a control gene (31).

Acknowledgements

We thank Dr A. Simonsen for discussion, Dr S. Lichtenthaler (TUM Munich, Germany) for the gift of anti-TMEM59 antibodies and TMEM59-HA plasmid, Drs B. Goud (Institut Curie, France) and M.T. Damiani (Mendoza, Argentina) for supplying Rab constructs and anti-Rab6 antibody (B.G.), Dr. G. Zhong (San Antonio, Texas) for anti-CT813 antibodies. We also thank Dr. E. Morel (INEM, France) for providing the GFP-ATG16L1 constructs, Dr. Laurent Boyer (Nice, France) for the NOD constructs and Dr. P Cossart (Institut Pasteur, France) for the TLR2 vector. We thank Thibault Chaze (Proteomics platform Institut Pasteur) for the analysis of the pull-down experiments. This work was supported by an ERC Starting Grant (NUChLEAR N°282046), and by a grant from the Pasteur-Weizmann Collaborative Research Funds. DH was funded by the ERC and by the Fondation pour la Recherche Médicale (SPF20170938695).

Declaration of interest

The authors declare no competing interests.

References

1. Brunham RC & Rey-Ladino J (2005) Immunology of *Chlamydia* infection: Implications for a *Chlamydia trachomatis* vaccine. *Nature Reviews Immunology* 5(2):149-161.
2. Triboulet S & Subtil A (2019) Make It a Sweet Home: Responses of Chlamydia trachomatis to the Challenges of an Intravacuolar Lifestyle. *Microbiol Spectr* 7(2).
3. Damiani MT, Tudela JG, & Capmany A (2014) Targeting eukaryotic Rab proteins: a smart strategy for chlamydial survival and replication. *Cellular Microbiology* 16(9):1329-1338.
4. Elwell C, Mirrashidi K, & Engel J (2016) *Chlamydia* cell biology and pathogenesis. *Nat Rev Microbiol* 14(6):385-400.
5. Cossé MM*, et al.* (2018) The Loss of Expression of a Single Type 3 Effector (CT622) Strongly Reduces *Chlamydia trachomatis* Infectivity and Growth. *Front Cell Inf Microbiol* 8(145):145.
6. Ohsumi Y (2014) Historical landmarks of autophagy research. *Cell Res.* 24(1):9-23.
7. Fletcher K*, et al.* (2018) The WD40 domain of ATG16L1 is required for its non-canonical role in lipidation of LC3 at single membranes. *The EMBO Journal* 37(4):e97840-97817.
8. Cadwell K & Debnath J (2018) Beyond self-eating: The control of nonautophagic functions and signaling pathways by autophagy-related proteins. *J. Cell Biol.* 217(3):813-822.
9. Lystad AH*, et al.* (2019) Distinct functions of ATG16L1 isoforms in membrane binding and LC3B lipidation in autophagy-related processes. *Nat Cell Biol* 21:372-383.
10. Sorbara MT*, et al.* (2013) The Protein ATG16L1 Suppresses Inflammatory Cytokines Induced by the Intracellular Sensors Nod1 and Nod2 in an Autophagy-Independent Manner. *Immunity* 39(5):858-873.
11. Bajagic M, Archna A, Büsing P, & Scrima A (2017) Structure of the WD40-domain of human ATG16L1. *Protein Sci.* 26(9):1828-1837.
12. Boada-Romero E*, et al.* (2013) TMEM59 defines a novel ATG16L1-binding motif that promotes local activation of LC3. *The EMBO Journal* 32(4):566-582.
13. Slowicka K*, et al.* (2019) Physical and functional interaction between A20 and ATG16L1-WD40 domain in the control of intestinal homeostasis. *Nature communications* 10(1):1834.
14. Al-Younes HM*, et al.* (2011) Autophagy-independent function of MAP-LC3 during intracellular propagation of *Chlamydia trachomatis*. *Autophagy* 7(8):814-828.
15. Vromman F, Laverriere M, Perrinet S, Dufour A, & Subtil A (2014) Quantitative Monitoring of the *Chlamydia trachomatis* Developmental Cycle Using GFP-Expressing Bacteria, Microscopy and Flow Cytometry. *PLoS One* 9(6):e99197.
16. Ullrich S*, et al.* (2010) The novel membrane protein TMEM59 modulates complex glycosylation, cell surface expression, and secretion of the amyloid precursor protein. *J. Biol. Chem.* 285(27):20664-20674.
17. Rzomp KA, Scholtes LD, Briggs BJ, Whittaker GR, & Scidmore MA (2003) Rab GTPases are recruited to Chlamydial inclusions in both a species-dependent and species-independent manner. *Infect. Immun.* 71(10):5855-5870.
18. Gambarte Tudela J*, et al.* (2015) The late endocytic Rab39a GTPase regulates the interaction between multivesicular bodies and chlamydial inclusions. *J. Cell Sci.* 128(16):3068-3081.

19. Rejman Lipinski A*, et al.* (2009) Rab6 and Rab11 regulate *Chlamydia trachomatis* development and golgin-84-dependent Golgi fragmentation. *PLoS Pathog* 5(10):e1000615.
20. Capmany A & Damiani MaT (2010) *Chlamydia trachomatis* Intercepts Golgi-Derived Sphingolipids through a Rab14-Mediated Transport Required for Bacterial Development and Replication. *PLoS ONE* 5(11):e14084.
21. Rogalski AA & Singer SJ (1984) Associations of elements of the Golgi apparatus with microtubules. *J. Cell Biol.* 99(3):1092-1100.
22. Jain BP & Pandey S (2018) WD40 Repeat Proteins: Signalling Scaffold with Diverse Functions. *The protein journal* 37(5):391-406.
23. Boncompain G & Weigel AV (2018) Transport and sorting in the Golgi complex: multiple mechanisms sort diverse cargo. *Curr. Opin. Cell Biol.* 50:94-101.
24. Hampe J*, et al.* (2006) A genome-wide association scan of nonsynonymous SNPs identifies a susceptibility variant for Crohn disease in ATG16L1. *Nat. Genet.* 39:207.
25. Murthy A*, et al.* (2014) A Crohn's disease variant in Atg16l1 enhances its degradation by caspase 3. *Nature* 506(7489):456-462.
26. Matsuzawa-Ishimoto Y, Hwang S, & Cadwell K (2018) Autophagy and Inflammation. *Annu. Rev. Immunol.* 36:73-101.
27. Cadwell K*, et al.* (2008) A key role for autophagy and the autophagy gene Atg16l1 in mouse and human intestinal Paneth cells. *Nature* 456(7219):259-263.
28. Gao P*, et al.* (2017) The Inflammatory Bowel Disease–Associated Autophagy Gene Atg16L1T300A Acts as a Dominant Negative Variant in Mice. *The Journal of Immunology* 198:2457-2467.
29. Ran FA*, et al.* (2013) Genome engineering using the CRISPR-Cas9 system. *Nature Protocols* 8(11):2281-2308.
30. Gehre L*, et al.* (2016) Sequestration of host metabolism by an intracellular pathogen. *Elife* 5:e12552.
31. Schmittgen TD & Livak KJ (2008) Analyzing real-time PCR data by the comparative CT method. *Nature Protocols* 3(6):1101-1108.

Figure Legends

Figure 1: TaiP binds directly to ATG16L1 through its carboxy-terminal domain to promote *C. trachomatis* infection

A) HeLa cells were co-transfected with Flag-CT622 and the indicated GFP-tagged construct for 24 hrs, lysed, and immunoprecipitation (IP) was performed with anti-Flag coupled beads. Proteins were separated on SDS-PAGE, transferred on a PVDF membrane and probed with the indicated antibody (IB : immunoblot). An aliquot of each cell lysate was loaded on a separate gel to visualize the expression of Flag-CT622 and of each of the GFP-tagged proteins (input, left panels).

B) Same as in A, using full-length CT622 or constructs corresponding to the N-terminal (CT622^{Nterm}, amino acids 1-345) or C-terminal (CT622^{Cterm}, amino acids 346-647).

C) HeLa cells were infected for 35 h with *Ctr*$^{\Delta ct622+CT622\text{-}Flag}$ bacteria, lysed, and IP was performed with anti-Flag coupled beads. Proteins were separated on SDS-PAGE, transferred on a PVDF membrane and probed with anti-Flag and anti-ATG16L1 antibody.

D) Recombinant ATG16L1 (100 nM) was incubated with recombinant GST-CT622 or GST-CT622^{Nterm} (100 nM) for 60 min at 4°C before performing GST-pulldown (PD) using glutathione beads. Pulled-down fractions were analyzed by western blot as in A. GST-CT622^{Nterm}, used here as a negative control, shows the level of non-specific ATG16L1 binding to the beads. ATG16L1 was pulled-down together with TaiP, demonstrating that the interaction is direct. The experiment shown is representative of three independent experiments.

E)Quantification of the effect of knocking-out *atg16l1* on inclusion size. WT or *atg16l1* KO cells seeded on coverslips were infected with either *Ctr*^{WT}, *Ctr*$^{\Delta taiP}$ or *Ctr*$^{\Delta taiP+TaiP\text{-}Flag}$ for 20 hrs at MOI=0.2. After fixation, infected cells were permeabilized and the inclusion membrane was stained with antibodies against the inclusion protein Cap1. The area of inclusion was measured using imageJ software. The dot-plot shows the median ± SD of 3 independent experiments (N>50 in total) and displays the P-values of the Student's t tests. The right panel shows the absence of ATG16L1 in *atg16l1* KO whole cell lysates probed by western blot with anti-ATG16L1 antibodies. ACTIN immunoblot serves as a loading control.

F) Quantification of the effect of TaiP expression on inclusion size. Cells were transfected with constructs for Flag-CymR or Flag-TaiP for 24 hours before being infected with *Ctr* or $Ct^{\Delta taiP}$. The cells were fixed 20 hrs post infection, permeabilized and the inclusion membrane was stained with antibodies against the inclusion protein Cap1. The area of inclusion was measured using imageJ software. The dot-plot displays the median ± SD of 3 independent experiments (N>50 in total) and displays the P-values of the Student's t test.

Figure 2: TaiP targets ATG16L1's WD40 domain.

A) Schematic representation of ATG16L1 structure including the coiled-coil domain (C.C.), the WD40 domain (WD40). The binding sites to ATG5, WIPI2B and FIP200 are highlighted, along with the serine phosphorylated by ULK1. WD40 binding partners are indicated on the right.

B) WT or *atg16l1* KO HeLa cells seeded on coverslips were transfected with the indicated constructs for 24 hours. Cells were then infected with $Ctr^{\Delta taiP}$ for 20 hours at MOI=0.2, before being fixed, permeabilized and the inclusion membrane was stained with antibodies against the inclusion protein Cap1. The graph displays the median ± SD of 3 independent experiments (N>50 cells in total) and the P-values of the Student's t test.

C) WT and HeLa cells were infected with either Ctr^{WT} or $Ctr^{\Delta taiP}$ for 20 hours, before fixation, permeabilization and immunostaining with antibodies against LC3B and the bacterial inclusion protein Cap1. LC3B is localized at the inclusion membrane independently of TaiP or ATG16L1. Scale bar: 10 µm. The dot plot displays the median intensity of LC3B staining at the inclusion membrane (N>10 cells from 3 independent experiments). Student's t tests showed no significant difference.

D) Lysates from *atg16l1* KO cells transfected with either GFP-ATG16L1 or GFP-$ATG16L1^{1-319}$ were incubated with 100 pmol of recombinant GST-TaiP for 1h at 4°C, before performing a GST-pull-down using Glutathione beads. Fractions were analyzed like in Fig 1A. ATG16L1 was no longer pulled-down withTaiP when its WD40 domain was deleted.

E) *atg16l1* KO Hela cells were co-transfected with Flag-TaiP and either GFP-ATG16L1 or GFP-$ATG16L1^{1-319}$. The cells were fixed 24 hrs later, permeabilized and stained with anti-

672 Flag antibodies. In the absence of the WD40 domain Flag-TaiP was no longer recruited to
673 ATG16L1 puncta. Scale bar: 10 µm.
674
675 **Figure 3: TaiP blocks the TMEM59/ATG16L1 complex to promote C*. trachomatis*
676 *i*nclusion expansion.**
677 **A)** Cells transfected with the indicated siRNA were infected with *Ct*$^{\Delta taiP}$ the following day
678 at MOI=0.2. Cells were fixed 20 hrs later, permeabilized and the inclusion membrane was
679 stained with anti-Cap1 antibodies. Inclusion areas were measured using imageJ software.
680 The Box and whiskers plots represent the median area and 90th percentile of intracellular
681 inclusions (N>50 cells from 3 independent experiments). Statistical analysis was performed
682 using a one -way anova test with a Dunnett's multiple comparison test to siCtrl.
683 **B)** Cells transfected with the indicated plasmids were infected or not 12 h later with *Ct*^{WT},
684 *Ct*$^{\Delta taiP}$ or *Ctr*$^{\Delta taiP+TaiP\text{-}Flag}$ bacteria at MOI=1. Cells were lysed 30 h later, and IP was performed
685 with anti-HA coupled beads. Proteins were separated on SDS-PAGE, transferred on a PVDF
686 membrane and probed with the indicated antibodies.
687 **C)** Lysates from cells expressing HA-TMEM59, or GFP-ATG16L1, were mixed in the
688 presence of 100 pmol of GST-TaiP or GST-TaiP^{Nterm} (for negative control) for 90 min at 4^{o}C in
689 a finale voume of 1.5 ml. TMEM59 was immunoprecipitated with anti-HA coupled beads and
690 the levels of GFP-ATG16L1 in the IP fraction was analyzed by western blot. Immunoblots of
691 the input fractions show the expression of each individual protein and represents 1.5 % of the
692 total reaction and comassie staining shows purified GST-TaiP and GST-TaiP^{Nterm}. The
693 histogram on the right displays the mean ±SD of three independent experiments and the P-
694 value of the Student's t test. Addition of GST-TaiP decreased the amount of GFP-ATG16L1
695 that co-immunoprecipitated with HA-TMEM59 by about 50%.
696 **D)** HeLa cells were co-transfected with Flag-TaiP, Flag-TaiP^{D480A} and GFP-ATG16L1
697 constructs for 24 h, lysed, and immunoprecipitation (IP) was performed with anti-Flag
698 antibody. Proteins were separated on SDS-PAGE, transferred on a PVDF membrane and
699 probed with the indicated antibody. An aliquot of each cell lysate was loaded on separate
700 gels to visualize the expression of the tagged proteins (input). Quantification on the right
701 shows the decrease in the amount of ATG16L1 that co-immunoprecipitates with Flag-

TaiP^{D480A} compared to Flag-TaiP. Statistical analysis was performed using Student's unpaired t test, n=4.

E) Quantification of the average inclusion size in cells expressing Flag-CymR, Flag-TaiP and Flag-TaiP^{D480A}. Cells were transfected for 24 hrs before they were infected for 20 hrs with *Ctr*$^{\Delta taiP}$ at MOI=0.2. After fixation and permeabilization inclusions were stained using antibodies against Cap1. Inclusion areas were measured using imageJ software. The dot-plot shows the median± SD of 3 independent experiments (N>50 cells in each experiment) and displays the P-values of the Student's t test.

Figure 4: TaiP redirects Rab6-positive vesicular traffic to the inclusion .

A) HeLa cells were co-transfected with Flag-TaiP and the indicated GFP-tagged Rab constructs for 24 hours. Cells were lysed, and immunoprecipitation (IP) was performed with anti-GFP antibody. Proteins were separated on SDS-PAGE, transferred to a PVDF membrane and probed with the indicated antibody (IB : immunoblot). An aliquot of each cell lysate was loaded on a separate gel to visualize the expression of Flag-TaiP and of each of the GFP-tagged proteins (input panels).

B) HeLa cells were co-transfected with the indicated constructs for 24 hrs and analyzed as in B.

C) Wild type and *atg16l1* KO cells were transfected as indicated and infected with *Ctr*^{WT} or *Ctr*$^{\Delta taiP}$ the following day at MOI=0.2. Cells were fixed 20 hrs post infection, permeabilized, and the inclusion membrane was stained with anti-Cap1 antibodies. Inclusion areas were measured using imageJ software. The Box and whiskers plots display the median area of intracellular inclusions (N>50 cells from 3 independent experiments). Statistical analysis was performed using a one-way anova with a Dunnett's multiple comparison test to siCtrl in WT HeLa. The inset shows the efficacy of the siRNA against Rab6 at silencing Rab6 expression probed by western blot.

D) Wild type and *atg16l1* KO cells were infected with *Ctr*^{WT} or *Ctr*$^{\Delta taiP}$ the following day at MOI=0.2. 20 h after infection the cells were treated with 10 nM nocodazole, and incubated further for 60 min before fixation. After permeabilization the cells were stained with rabbit antibodies against endogenous Rab6 and mouse antibodies against the inclusion membrane protein CT813. Representative images are shown, scale bar: 10 µm. The Box and whiskers

plot displays the median intensity of the Rab6 staining at the inclusion periphery, relative to its cytosolic intensity (N>50 cells from 3 independent experiments, see Methods for details). Statistical analysis was performed using Student's t test.

Figure 5: TaiP disrupts the ATG16L1-controlled traffic of Rab6-positive vesicles towards TMEM59-positive compartments.

A) Model.*a.* In unifected cells, ATG16L1's binding to TMEM59 facilitates the supply of Rab6 positive veiscles to TMEM59 positive compartments. *b*. In cells infected with *Ctr*^{WT}, TaiP secretion by the bacteria prevents ATG16L1/TMEM59 interaction, and Rab6 positive vesicles are hijacked by the inclusion. *c*. In the absence of TaiP, the bacteria lose access to this pool of vesicles. *Ctr*$^{\Delta taiP}$ inclusions are smaller, as they only rely on alternative membrane sources. *d*. Silencing ATG16L1 or TMEM59 expression reverts this phenotype.

B) Wild type and *atg16l1* KO Hela cells were co-transfected with the indicated plasmids. One day later, the cells were lysed, and immunoprecipitation (IP) was performed with anti-HA coupled beads. Proteins were separated on SDS-PAGE, transferred to a PVDF membrane and probed with the indicated antibody. GFP-Rab6 co-immunoprecipitated with TMEM59 only in cells expressing ATG16L1. The use of cells that do not express HA-TMEM59 allows to measure the level of non-specific association of GFP-Rab6 to the beads.

Figure1

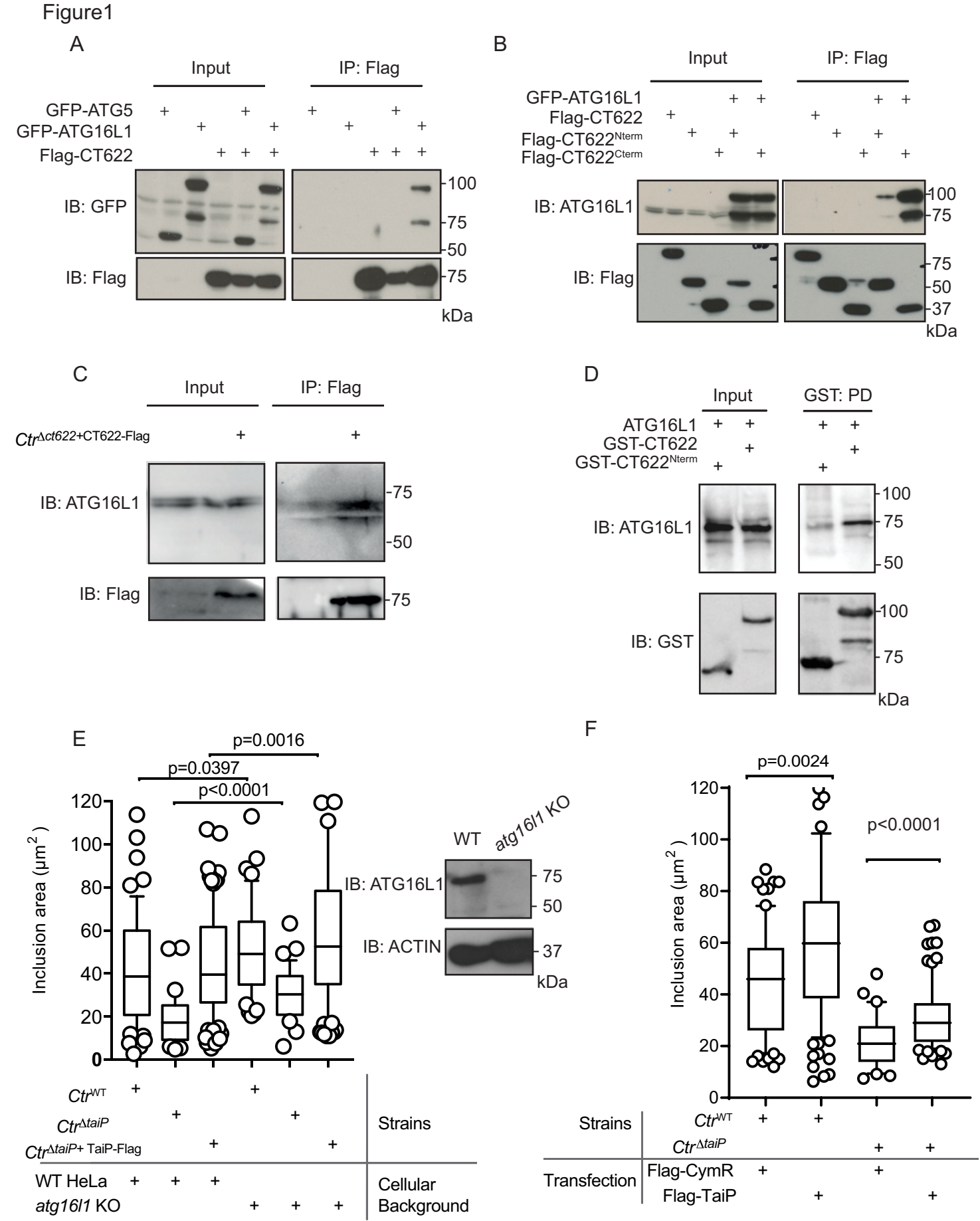
A
Input
IP: Flag
GFP-ATG5
GFP-ATG16L1
Flag-CT622
IB: GFP
IB: Flag
100
75
50
75
kDa
B
Input
IP: Flag
GFP-ATG16L1
Flag-CT622
Flag-CT622Nterm
Flag-CT622Cterm
IB: ATG16L1
IB: Flag
100
75
75
50
37
kDa
C
Input
IP: Flag
CtrΔct622+CT622-Flag
IB: ATG16L1
IB: Flag
75
50
75
D
Input
GST: PD
ATG16L1
GST-CT622
GST-CT622Nterm
IB: ATG16L1
IB: GST
100
75
50
100
75
kDa
E
p=0.0016
p=0.0397
p<0.0001
Inclusion area (μm2)
120
100
80
60
40
20
0
WT
atg16l1 KO
IB: ATG16L1
IB: ACTIN
75
50
37
kDa
CtrWT
CtrΔtaiP
CtrΔtaiP+ TaiP-Flag
Strains
WT HeLa
atg16l1 KO
Cellular Background
F
p=0.0024
p<0.0001
Inclusion area (μm2)
120
100
80
60
40
20
0
Strains
CtrWT
CtrΔtaiP
Transfection
Flag-CymR
Flag-TaiP

Figure2

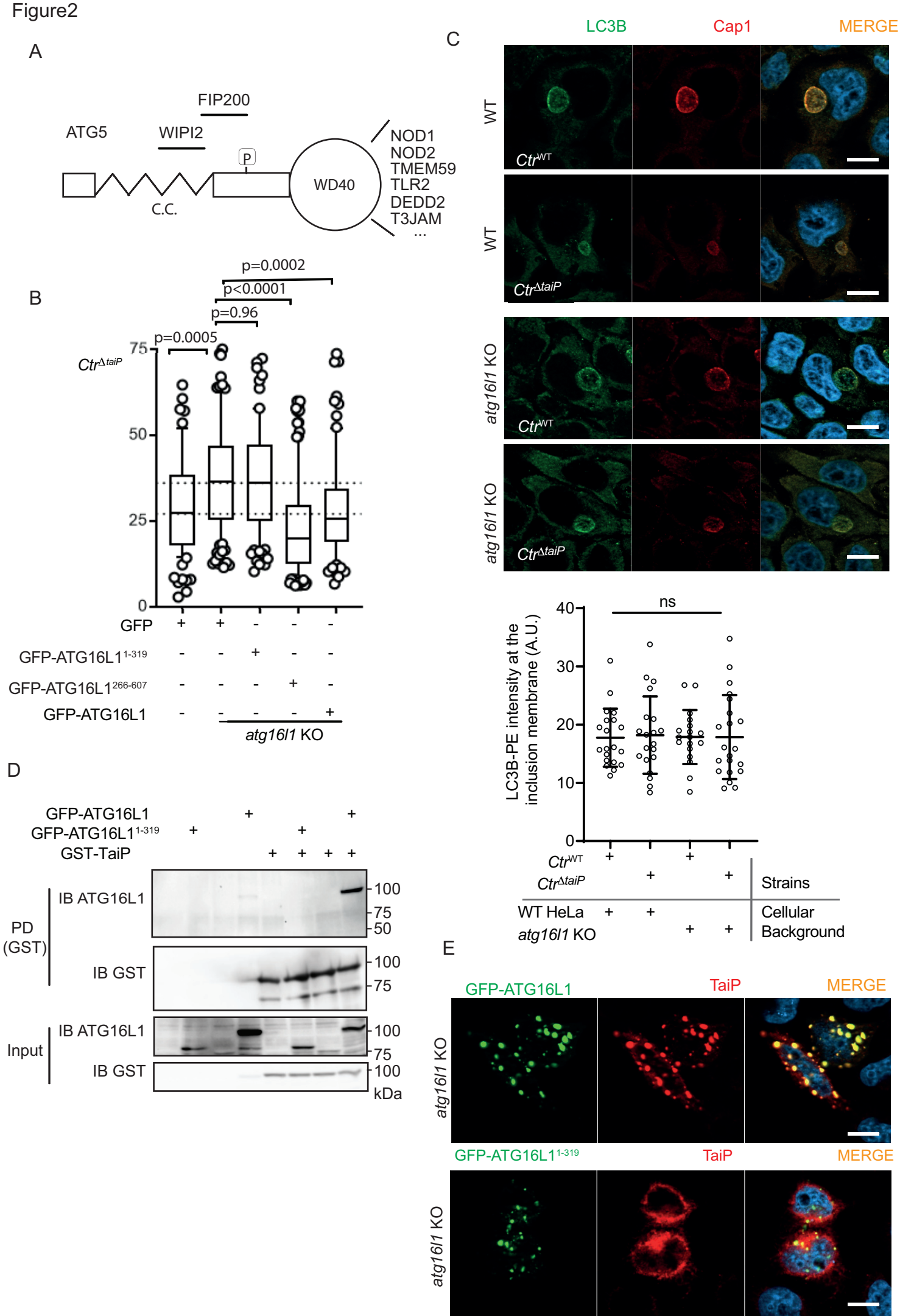
A
FIP200
ATG5
WIPI2
P
WD40
C.C.
NOD1
NOD2
TMEM59
TLR2
DEDD2
T3JAM
...
B
p=0.0002
p<0.0001
p=0.96
p=0.0005
CtrΔtaiP
75
50
25
0
GFP + + - - -
GFP-ATG16L1 1-319 - - + - -
GFP-ATG16L1 266-607 - - - + -
GFP-ATG16L1 - - - - +
atg16l1 KO
C
LC3B
Cap1
MERGE
WT
CtrWT
WT
CtrΔtaiP
atg16l1 KO
CtrWT
atg16l1 KO
CtrΔtaiP
LC3B-PE intensity at the inclusion membrane (A.U.)
ns
40
30
20
10
0
CtrWT + +
CtrΔtaiP + +
Strains
WT HeLa + +
atg16l1 KO + +
Cellular Background
D
GFP-ATG16L1 + +
GFP-ATG16L1 1-319 + +
GST-TaiP + + + +
PD (GST)
IB ATG16L1
IB GST
Input
IB ATG16L1
IB GST
100
75
50
100
75
100
75
100
kDa
E
GFP-ATG16L1
TaiP
MERGE
atg16l1 KO
GFP-ATG16L1 1-319
TaiP
MERGE
atg16l1 KO

Figure 3

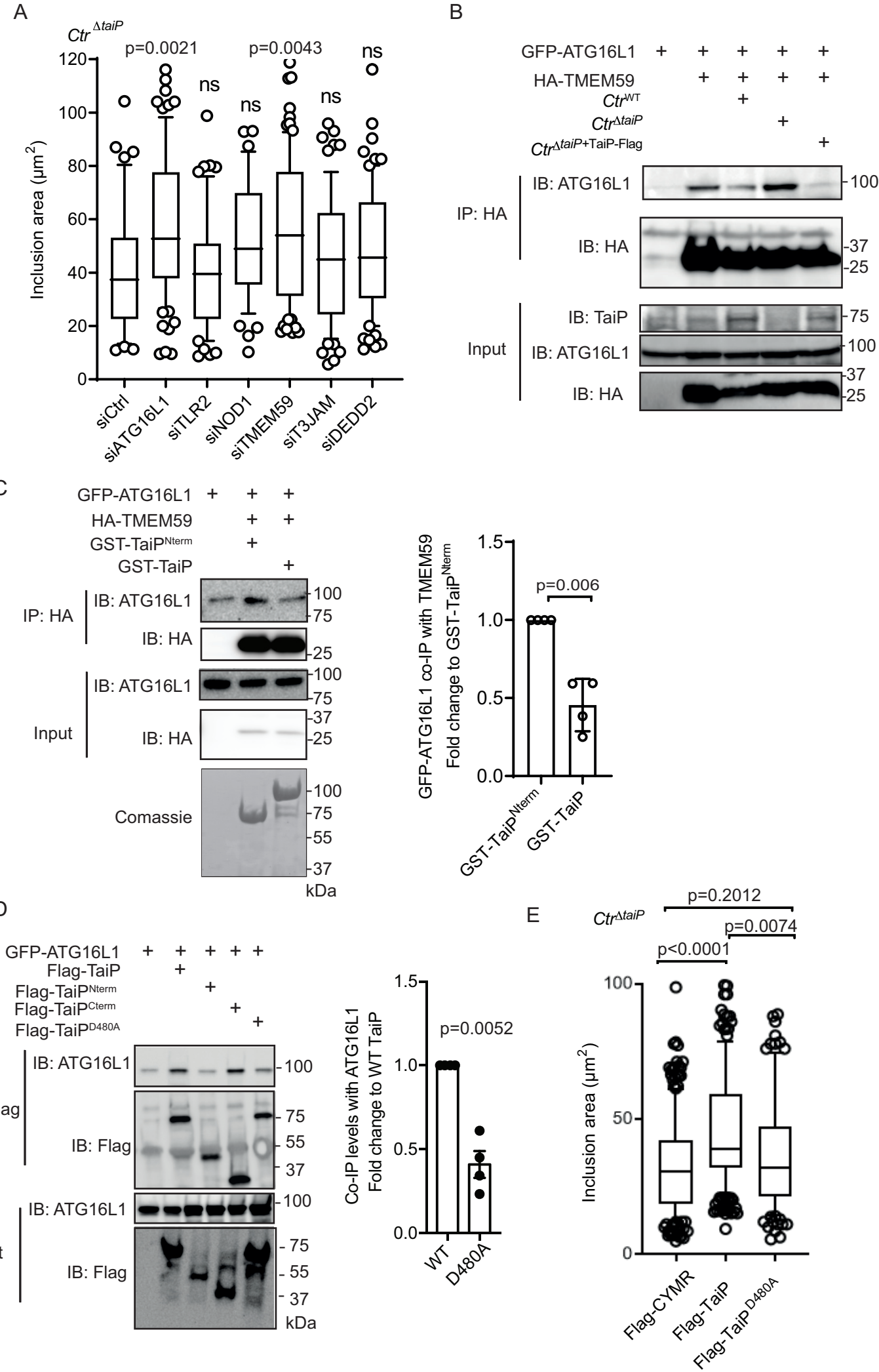
A
Ctr ΔtaiP
p=0.0021
p=0.0043
ns
ns
ns
ns
Inclusion area (μm2)
120
100
80
60
40
20
0
siCtrl
siATG16L1
siTLR2
siNOD1
siTMEM59
siT3JAM
siDEDD2
B
GFP-ATG16L1 + + + + +
HA-TMEM59 + + + +
CtrWT +
CtrΔtaiP +
CtrΔtaiP+TaiP-Flag +
IP: HA
IB: ATG16L1
IB: HA
Input
IB: TaiP
IB: ATG16L1
IB: HA
100
37
25
75
100
37
25
C
GFP-ATG16L1 + + +
HA-TMEM59 + +
GST-TaiPNterm +
GST-TaiP +
IP: HA
IB: ATG16L1
IB: HA
Input
IB: ATG16L1
IB: HA
Comassie
100
75
25
100
75
37
25
100
75
55
37
kDa
GFP-ATG16L1 co-IP with TMEM59
Fold change to GST-TaiPNterm
p=0.006
1.5
1.0
0.5
0.0
GST-TaiPNterm
GST-TaiP
D
GFP-ATG16L1 + + + + +
Flag-TaiP +
Flag-TaiPNterm +
Flag-TaiPCterm +
Flag-TaiPD480A +
IP: Flag
IB: ATG16L1
IB: Flag
Input
IB: ATG16L1
IB: Flag
100
75
55
37
100
75
55
37
kDa
Co-IP levels with ATG16L1
Fold change to WT TaiP
p=0.0052
1.5
1.0
0.5
0.0
WT
D480A
E
CtrΔtaiP
p=0.2012
p=0.0074
p<0.0001
Inclusion area (μm2)
100
50
0
Flag-CYMR
Flag-TaiP
Flag-TaiP D480A

Figure 4

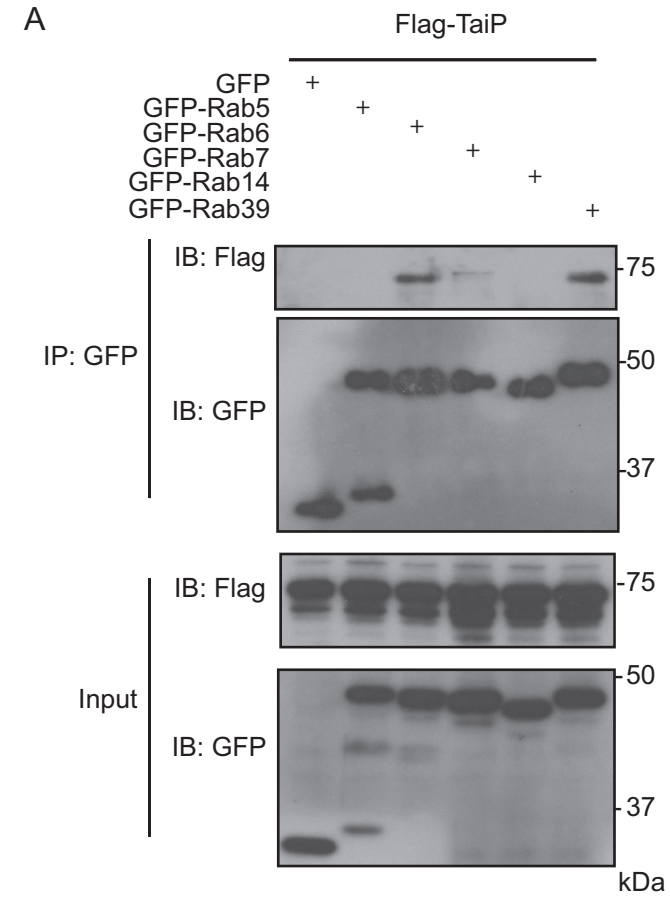
A
Flag-TaiP
GFP
GFP-Rab5
GFP-Rab6
GFP-Rab7
GFP-Rab14
GFP-Rab39
IP: GFP
IB: Flag
IB: GFP
Input
IB: Flag
IB: GFP
75
50
37
75
50
37
kDa

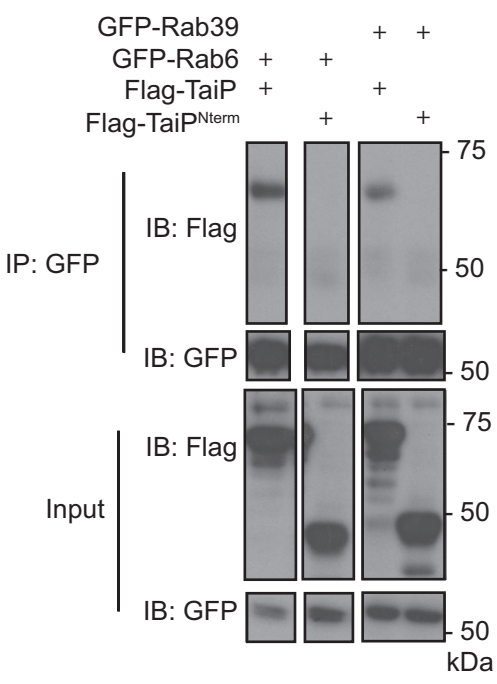
B
GFP-Rab39
GFP-Rab6
Flag-TaiP
Flag-TaiPNterm
IP: GFP
IB: Flag
IB: GFP
Input
IB: Flag
IB: GFP
75
50
50
75
50
50
kDa

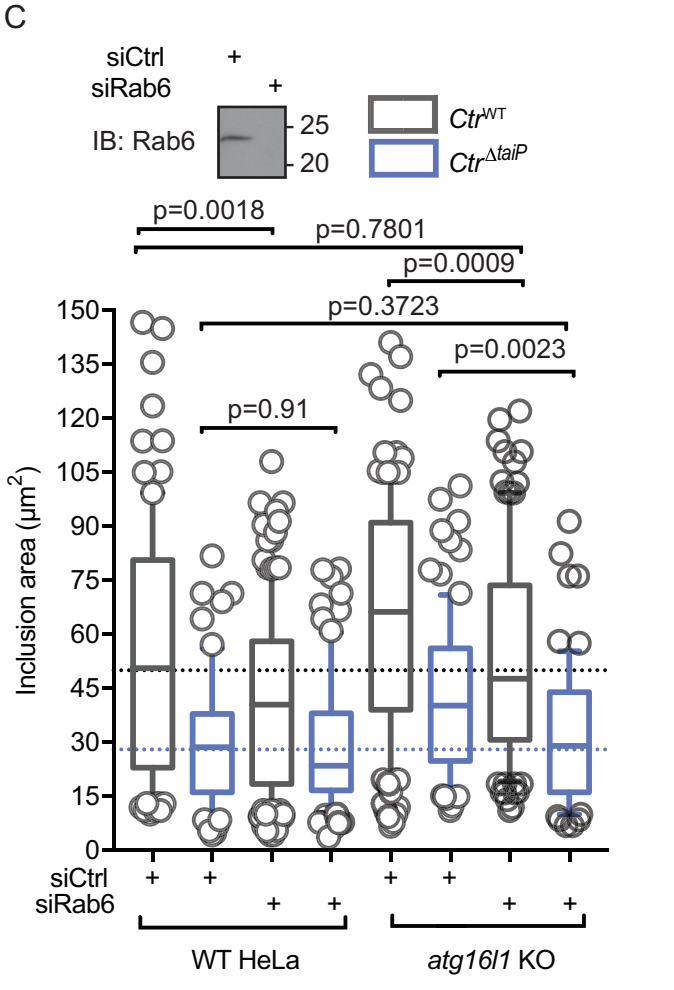
C
siCtrl
siRab6
IB: Rab6
25
20
CtrWT
CtrΔtaiP
p=0.0018
p=0.7801
p=0.0009
p=0.3723
p=0.0023
p=0.91
Inclusion area (µm2)
150
135
120
105
90
75
60
45
30
15
0
siCtrl
siRab6
WT HeLa
atg16l1 KO

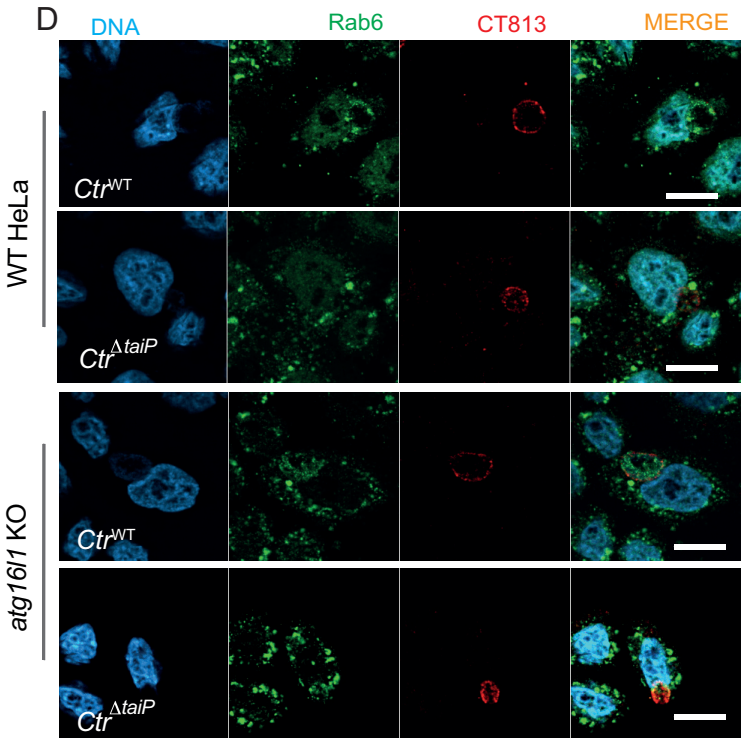
D
DNA
Rab6
CT813
MERGE
WT HeLa
atg16l1 KO
CtrWT
CtrΔtaiP
CtrWT
CtrΔtaiP

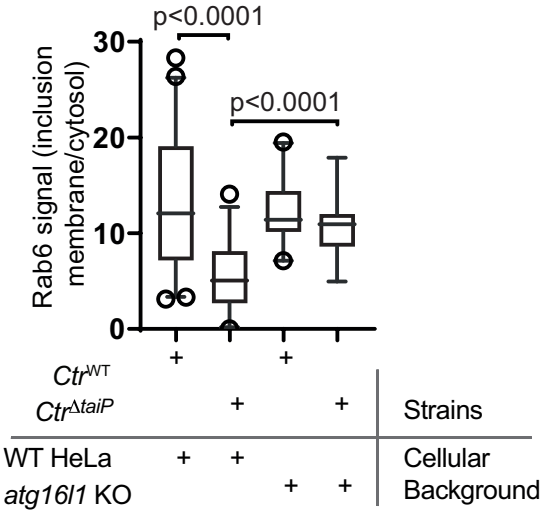
p<0.0001
p<0.0001
Rab6 signal (inclusion membrane/cytosol)
30
20
10
0
CtrWT
CtrΔtaiP
Strains
WT HeLa
atg16l1 KO
Cellular Background

Figure5

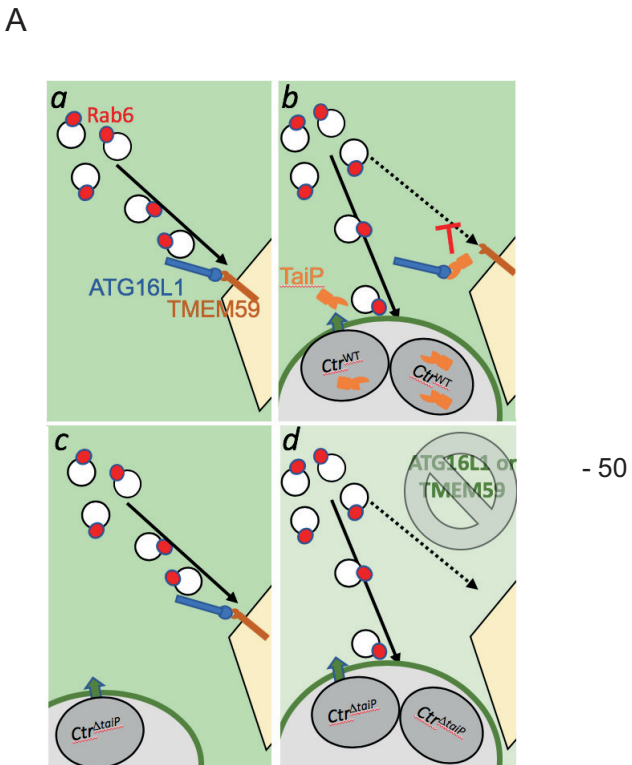
A
a
Rab6
ATG16L1
TMEM59
b
TaiP
Ctr^WT
Ctr^WT
c
Ctr^ΔtaiP
d
ATG16L1 or TMEM59
Ctr^ΔtaiP
Ctr^ΔtaiP
- 50

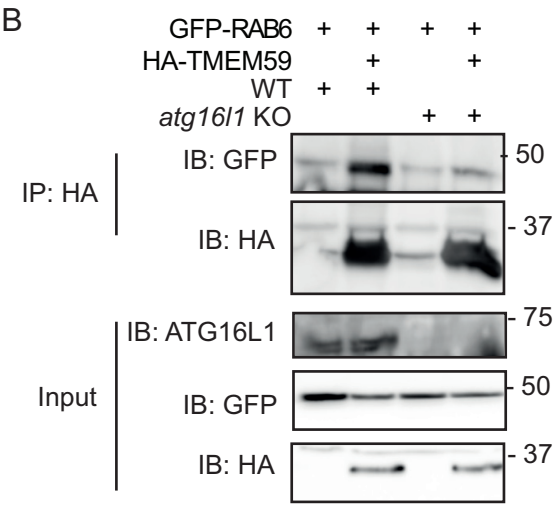
B
GFP-RAB6 + + + +
HA-TMEM59 + +
WT + +
atg16l1 KO + +
IP: HA
IB: GFP
IB: HA
Input
IB: ATG16L1
IB: GFP
IB: HA
50
37
75
50
37